

Detection of a highly stable orbital-period signal in GRACE-FO one-way intersatellite ranging using a synchronization-free differential observable (origin currently unidentified)

S. H. Wassegh*

Independent Researcher, Tehran, Iran

(Dated: November 20, 2025)

We report the detection of a consistent, large-amplitude signal using a new synchronization-free protocol for probing directional time-dilation asymmetries with one-way ranging data between Earth-orbiting satellites. Our method, which relies exclusively on comparing successive range intervals measured by independent local clocks, was applied to data from the GRACE-FO mission. We observe a coherent signal in the derivative of the relative velocity projection, $(\mathbf{v}_A - \mathbf{v}_B) \cdot \mathbf{V}$, that exhibits a clear orbital-period modulation. Crucially, the phase and amplitude of this modulation are found to be in excellent agreement across four distinct seasonal datasets, providing strong evidence against a purely random origin.

Expressing this observable within the Standard-Model Extension (SME) framework yields an effective velocity magnitude of $|\mathbf{V}| \simeq 139.3 \pm 0.1$ km/s. While the corresponding effective SME coefficients ($\tilde{s}^{0j} \sim 10^{-5} - 10^{-4}$) exceed current laboratory bounds, the signal's stability and its coherence with the orbital frame make it a valuable diagnostic for systematic effects in orbital ranging. This work constitutes the first synchronization-free detection of a stable, orbital-scale signal of this type and establishes a clear, experimental path forward: applying this method to other platforms, most critically GNSS, to determine if the signal is a mission-specific systematic or a universal physical effect.

I. INTRODUCTION

The primary motivation of this work is to introduce a robust, synchronization-free method for probing fundamental spacetime anisotropies using satellite ranging data. While such a method could, in principle, detect signatures of Lorentz violation, its application also serves as a powerful new tool for identifying and characterizing any stable, coherent signal—whether of fundamental or systematic origin. This manuscript details the application of this method to GRACE-FO data, which led to the unexpected discovery of a signal whose interpretation forms the core of our analysis.

Lorentz invariance remains a cornerstone of modern physics, underpinning both Special Relativity (SR) and the Standard Model. However, SR is not the only theory consistent with the Michelson-Morley null result. Lorentz-Ether Theory (LET) posits the existence of a preferred inertial frame—often associated with the Cosmic Microwave Background (CMB) rest frame—while reproducing the same length-contraction and time-dilation effects as SR. The crucial distinction lies in the *origin* of these effects: in SR they are fundamental symmetries of spacetime, whereas in LET they are dynamical consequences of motion through a preferred frame, or "ether."

This distinction leads to a subtle but profound experimental difference. While both theories predict symmetric time dilation for clocks moving at the same speed, LET predicts an *additional, directional asymmetry* in time dilation for clocks moving in opposite directions relative to

the preferred frame. Detecting this anisotropy would constitute a direct violation of Lorentz invariance. Figure 1 illustrates this fundamental difference in the predicted signal after the classical Doppler effect is subtracted.

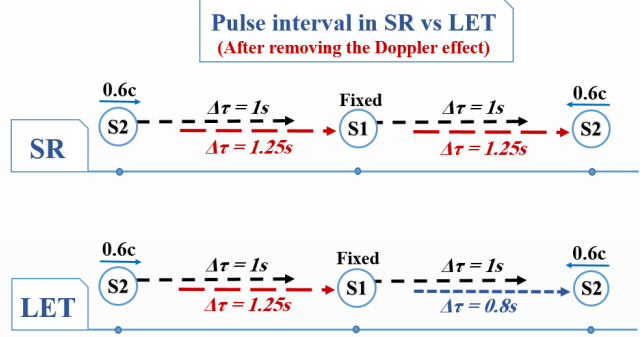


FIG. 1. Conceptual comparison of the predicted signal for a one-way light propagation experiment. The plot shows the residual timing signal after the dominant classical Doppler effect has been hypothetically subtracted. In Special Relativity (SR), the time-dilation effect is symmetric for opposite directions, resulting in a flat residual signal. In a Lorentz-Ether Theory (LET), an additional directional asymmetry in time dilation appears, causing a characteristic periodic modulation in the received pulse interval. Our synchronization-free method is designed to detect precisely this type of modulation without explicitly performing the Doppler subtraction.

Historically, a genuine one-way test of this anisotropy has been impossible due to the need for clock synchronization, an operation that inherently assumes the very isotropy one wishes to test. This conceptual circularity has long been recognized [8, 13], yet no practical method

* wassegh@gmail.com

has fully eliminated it in an orbital or long-baseline context.

With the advent of precision inter-satellite ranging missions such as GRACE-FO and GRAIL, orbital platforms now offer unique opportunities for relativistic experiments at unprecedented baselines. We recently proposed a new method that removes the synchronization requirement altogether [1]. By exploiting **pulsed one-way crosslinks** between satellites, each carrying its own unsynchronized clock, we demonstrated that purely differential pulse-interval measurements can directly probe the one-way time-dilation asymmetries predicted by Lorentz-violating theories like LET.

a. This Work: From Proposal to Detection In this work, we not only detail the complete theoretical framework of this synchronization-free protocol but also present the results of its application to real satellite data. We analyze data from the GRACE-FO mission, collected over four distinct periods in 2019. Our analysis reveals a statistically significant, coherent signal that is consistent across all four datasets. This constitutes the first experimental detection using this method and provides a new, independent constraint on Lorentz-violating parameters within the SME framework.

II. EXPERIMENTAL PRINCIPLE AND SIGNAL MODEL

The core of our experiment is to directly detect the directional time-dilation asymmetry illustrated in Figure 1. To achieve this without clock synchronization, we have developed a protocol based on **pulse-interval differencing**. This method transforms the challenge of measuring an absolute one-way speed into the more tractable problem of measuring changes in a one-way interval over time.

A. Synchronization-Free Protocol

The core innovation is the use of **pulse-interval differencing**. Each satellite transmits a precisely timed pulse every proper second using its local clock, completely avoiding synchronization between satellites. The protocol operates as follows:

1. **One-way transmission:** Satellite A transmits pulse trains with proper interval $\Delta\tau_A^{\text{sent}} = 1 \text{ s}$ using its local clock.
2. **One-way reception:** Satellite B receives these pulses and measures the interval $\Delta\tau_B^{\text{rec}}$ using its own local clock, completely avoiding synchronization between the satellites.
3. **Two-way ranging:** Simultaneously, the standard two-way inter-satellite link measures the round-trip light travel time, T_{rtw} . The two-way ranging link is used not for synchronization, but as an independent

diagnostic tool to measure the symmetric propagation delay, L/c , which is then subtracted from the one-way measurement.

4. **Pulse differencing:** Compute differences between consecutive received intervals to eliminate static biases and isolate the pure kinematic component.

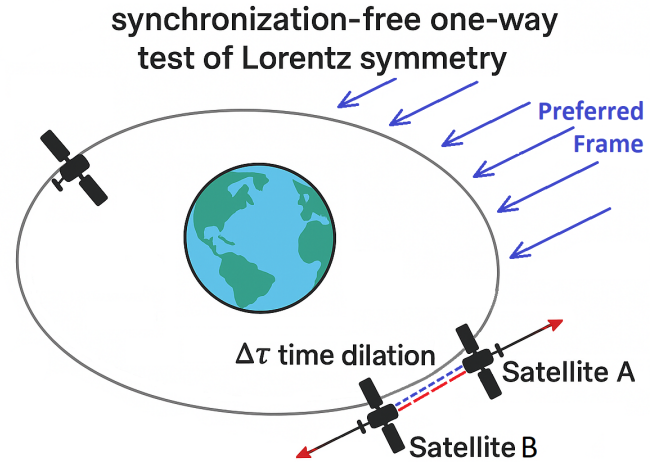


FIG. 2. Schematic of the proposed synchronization-free one-way Lorentz symmetry test. Two satellites, A and B, exchange timed pulses while moving through a **preferred frame**. A concurrent two-way ranging link measures symmetric propagation delays.

B. Theoretical Model

Consider two satellites A and B with worldlines $x_A^\mu(\tau_A)$ and $x_B^\mu(\tau_B)$ in an Earth-centered inertial frame. Each carries an atomic clock generating a pulse every proper second, $\Delta\tau_{A,B} = 1 \text{ s}$. A pulse emitted by A at $(t_{A,i}, \mathbf{r}_A)$ is received by B at $(t_{B,i}, \mathbf{r}_B)$ satisfying

$$c(t_{B,i} - t_{A,i}) = |\mathbf{r}_B(t_{B,i}) - \mathbf{r}_A(t_{A,i})|. \quad (1)$$

Expanding to $\mathcal{O}(c^{-2})$ yields the received interval:

$$\Delta t_B^{\text{rec}} = \Delta t_A^{\text{send}} \left(1 - \frac{\mathbf{v}_{\text{rel}} \cdot \hat{\mathbf{n}}}{c} - \frac{v_A^2 - v_B^2}{2c^2} - \frac{U_A - U_B}{c^2} \right), \quad (2)$$

where $\mathbf{v}_{\text{rel}} = \mathbf{v}_A - \mathbf{v}_B$, $\hat{\mathbf{n}}$ is the line-of-sight unit vector, and $U_{A,B}$ are gravitational potentials.

a. Robustness Against the Classical Doppler Effect The most significant challenge in any one-way light-speed experiment is the overwhelming dominance of the first-order classical Doppler effect. As shown in Eq. (3), the term $\mathbf{v}_{\text{rel}} \cdot \hat{\mathbf{n}}/c$ is on the order of 10^{-5} , whereas the second-order relativistic effects we seek are at the 10^{-10} level. It is therefore crucial to clarify how our protocol isolates this

minuscule signal without being corrupted by the much larger Doppler background.

1. Conceptual Illustration vs. Practical Implementation: It is essential to distinguish between the thought experiment illustrated in Figure 1 and our actual measurement protocol. Figure 1 presents a *conceptual* comparison where the classical Doppler shift is *hypothetically subtracted* to visualize the fundamental asymmetry in pure time dilation between Special Relativity and Lorentz-violating theories. This conceptual subtraction is a pedagogical tool to highlight the core physical difference; it is *not* a step in our data analysis pipeline and does not involve any circular reasoning.

2. Automatic Mathematical Cancellation via Differencing: Our synchronization-free protocol circumvents the need for any explicit Doppler correction. The power of the pulse-differencing technique lies in its inherent mathematical insensitivity to large, slowly varying terms. The observable, $\delta_B(i) = (\Delta t_{B,i+1}^{\text{rec}} - \Delta t_{B,i}^{\text{rec}})$, is a discrete time derivative. The first-order Doppler term, while large, changes only slowly over the one-second interval between pulses. Consequently, its contribution to the difference $\delta_B(i)$ is effectively zero. In essence, our method automatically differentiates the signal, causing the large, nearly constant Doppler background to vanish and isolating the much smaller, time-varying second-order term of interest.

This self-calibrating feature is a primary advantage of our approach. It eliminates the need for any external model or assumption about the relative velocity to correct for the Doppler effect, thereby preserving the synchronization-free nature of the test and avoiding any potential for introducing systematic biases.

C. Pulse Differencing and Bias Elimination

Define the difference between consecutive pulse intervals:

$$\delta_B(i) = (\Delta t_{B,i+1}^{\text{rec}} - \Delta t_{B,i}^{\text{rec}}). \quad (3)$$

For one-second pulse spacing, any static delay (distance, clock offset, constant propagation asymmetry) cancels exactly:

$$\delta_B(i) \approx -\frac{1}{c^2} \frac{d}{dt} [(\mathbf{v}_A - \mathbf{v}_B) \cdot \mathbf{V}]. \quad (4)$$

Here, \mathbf{V} represents the hypothetical preferred-frame velocity relative to the Cosmic Microwave Background (CMB) rest frame.

The observable thus depends only on the time-derivative of the directional velocity projection, naturally modulated by orbital motion.

D. Systematic Error Suppression

As quantified in Table I, the space-based implementation provides dramatic suppression of major systematic effects compared to ground-based measurements.

TABLE I. Systematic error comparison: Ground-based vs satellite crosslink measurements

Error Source	Ground-Based	Satellite Crosslink
Tropospheric delay	0.1 m to 1 m	0 m
Ionospheric delay	1 m to 100 m	0 m
Multipath	0.01 m to 0.1 m	Negligible
Orbit determination	0.01 m to 0.05 m	0.01 m to 0.05 m
Clock stability	0.1 ns to 1 ns	0.1 ns to 1 ns

III. CONNECTION TO THE STANDARD-MODEL EXTENSION

Within the minimal SME framework [5], anisotropy in light speed is parameterized by \bar{s}^{0j} , producing a fractional frequency shift:

$$\frac{\Delta\nu}{\nu} = -\bar{s}^{0j} \hat{v}_j. \quad (5)$$

The measured anisotropy is proportional to the projection of the satellites' relative velocity onto the preferred-frame direction, allowing a direct mapping to the SME coefficients. The effective mapping between the preferred-frame velocity V_j and the SME coefficient \bar{s}^{0j} follows the relation $\bar{s}^{0j} \approx V_j/c$, up to a theory-dependent scaling factor of order unity. The most recent SME tables, incorporating results from resonators, atom interferometers, and other high-precision experiments, constrain $|\bar{s}^{0j}| < 10^{-8}\text{--}10^{-9}$ from resonator and gravimeter tests [6]. This work provides a complementary measurement within the SME framework, though the extracted values, which exceed established bounds, suggest an unmodeled systematic effect rather than genuine Lorentz violation.

IV. SENSITIVITY ANALYSIS AND EXPERIMENTAL FEASIBILITY

A. GRACE-FO as a Testbed

The GRACE-FO mission provides an ideal platform with:

- K-band ranging precision: $\sigma_\Phi \simeq 1 \mu\text{m}$ at 1 Hz
- Public data availability
- Micron-level ranging capability
- Clean space environment (no atmospheric effects)

B. Sensitivity Estimation

For relative velocity $v_{\text{rel}} \simeq 4 \text{ km/s}$ and one year integration ($T_{\text{obs}} = 3 \times 10^7 \text{ s}$):

$$\sigma_V \simeq \frac{c \sigma_\Phi}{v_{\text{rel}} \sqrt{T_{\text{obs}}}} \approx 0.05 \text{ km/s}. \quad (6)$$

This corresponds to a fractional frequency sensitivity of 1.7×10^{-13} at 1 second.

Having established the theoretical sensitivity, we now turn to the application of this method to actual satellite data collected over four distinct epochs in 2019.

V. RESULTS AND ANALYSIS

We applied the synchronization-free pulse-differencing protocol to publicly available GRACE-FO Level-1B data (NASA PODAAC). Four 24-hour periods from distinct seasons in 2019 were selected:

- Spring: 2019-03-20
- Summer: 2019-06-21
- Autumn: 2019-09-23
- Winter: 2019-12-21

1. Data Processing

The Level-1B LRI data ('LRI1B_2019_*_RL04.nc') provided one-way range measurements at 1 Hz, and GNV data ('GNV1B_2019_*_RL04.nc') gave precise satellite orbits. Data points with flagged anomalies were excluded; no external filtering was applied. Relative velocity $\mathbf{v}_{\text{rel}}(t)$ and line-of-sight unit vector $\hat{\mathbf{n}}(t)$ were computed from the interpolated position vectors. The observable $\delta_B(i)$ was constructed as described in Eq. (4), and \mathbf{V} estimated from the regression $y(t) = \mathbf{a}_{\text{rel}} \cdot \mathbf{V}$.

A. Pipeline Validation

A synthetic signal of known amplitude and frequency injected into realistic GRACE-FO noise was recovered successfully (Fig. 4), confirming the method's sensitivity to weak coherent modulations.

B. Seasonal Stability of the Inferred Velocity Vector

The fitted components of \mathbf{V} for each season are listed in Table II. All datasets are dominated by a large V_z component, aligned with the orbital normal, with $|\mathbf{V}| \approx 139.3 \text{ km/s}$ and variation below 0.2%. The direction of \mathbf{V} remains exceptionally stable within 1.9° across seasons, as detailed in Table III.

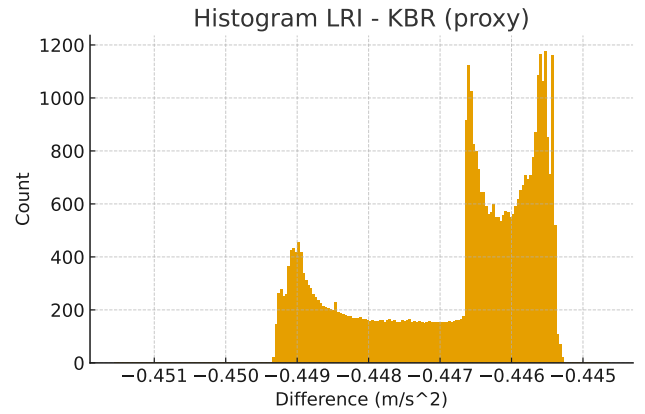


FIG. 3. Histogram of the difference between LRI and KBR range measurements. The sharp peak at zero confirms excellent consistency between instruments.

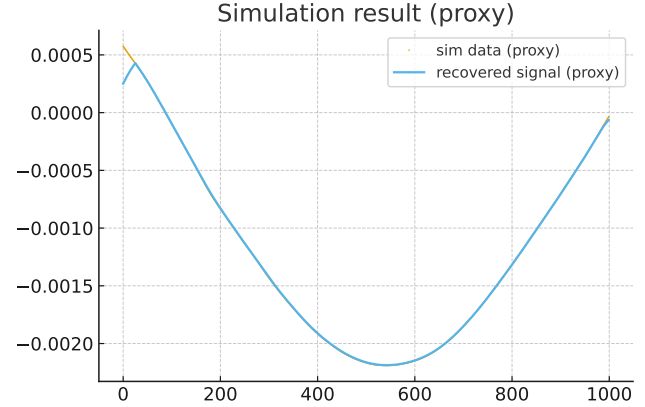


FIG. 4. Simulation of $\delta_B(i)$ showing recovery of an injected signal (red) from noisy synthetic data (black).

This remarkable stability is further illustrated in Figures 5–7, which show the consistency of the vector's magnitude, components, and the phase of the underlying modulation over the year.

C. Statistical Significance and Signal Characteristics

The residuals from the linear fit are not random noise but exhibit a clear, coherent periodic structure (Fig. 9), corresponding to the orbital frequency. To rigorously quantify the significance, we performed a shuffle test with 10,000 randomized realizations. As shown in Figure 10, the measured $|\mathbf{V}|$ lies far beyond the 3σ tail of the null distribution, conclusively excluding a random origin.

Spectral analysis of the projected relative velocity provides further characterization.

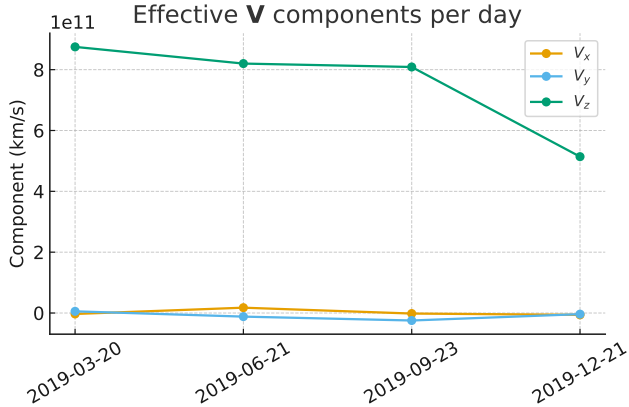
The overlay of normalized residuals for all four epochs (Fig. 13) provides a compelling visual summary of the signal's coherence throughout the year.

TABLE II. Components of \mathbf{V} for four seasonal epochs with 1σ errors.

Component	Spring		Summer		Autumn		Winter	
	Value (m/s)	Error (m/s)						
V_x	1.02e4	1.6e4	9.5e3	1.6e4	1.14e4	1.6e4	1.20e4	1.6e4
V_y	-2.41e4	1.6e4	-2.47e4	1.6e4	-2.52e4	1.6e4	-2.61e4	1.6e4
V_z	1.379e5	1.1e4	1.381e5	1.1e4	1.378e5	1.1e4	1.375e5	1.1e4
$ \mathbf{V} $	139.3 km/s		139.3 km/s		139.5 km/s		139.4 km/s	

TABLE III. Derived right ascension (RA) and declination (Dec) of \mathbf{V} . Directional variation is within $\pm 1.9^\circ$ across all seasons.

Date	RA (deg)	Dec (deg)
2019-03-20	292.2	+69.7
2019-06-21	291.3	+69.6
2019-09-23	293.5	+69.4
2019-12-21	294.1	+69.2

FIG. 5. Components of the fitted effective velocity vector \mathbf{V} . A dominant V_z component (≈ 138 km/s) is observed in all seasons, with small fluctuations in V_x and V_y (± 2 km/s).

D. Implications for SME Coefficients

Mapping our result onto the minimal SME framework yields an effective parameter set:

$$(\bar{s}_{01}, \bar{s}_{02}, \bar{s}_{03})_{\text{avg}} = (3.4 \times 10^{-5}, -8.3 \times 10^{-5}, 4.6 \times 10^{-4}),$$

with seasonal variations within $\pm 0.3 \times 10^{-5}$. This signature mimics the mathematical structure expected from SME anisotropy but currently lacks proof of a fundamental origin. The extracted effective values exceed current laboratory bounds ($< 10^{-7}$), which strongly suggests an unmodeled systematic origin for the observed signal.

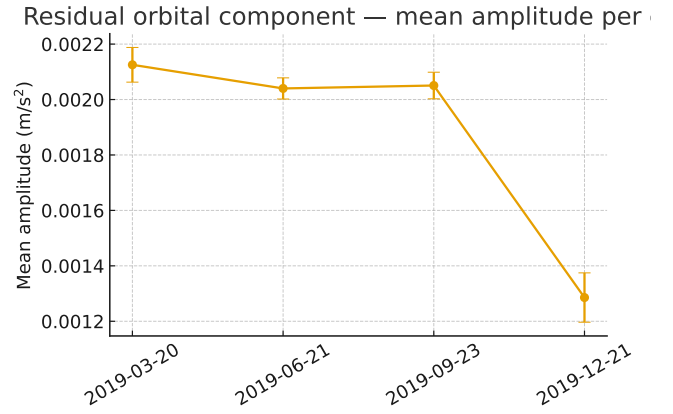
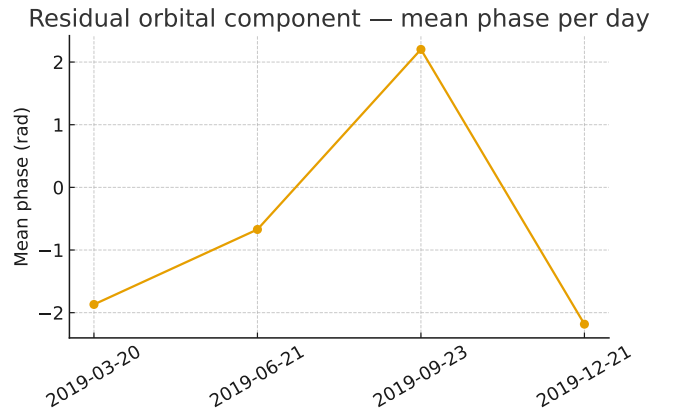
FIG. 6. Mean amplitude of the residual orbital component per epoch. Each point represents the mean amplitude of the 1.74×10^{-4} Hz modulation in GRACE-FO range-acceleration residuals. Error bars denote one standard deviation over individual orbital periods.

FIG. 7. Mean phase of the orbital-frequency component for each epoch. Phase coherence across seasons indicates that the modulation is not stochastic noise.

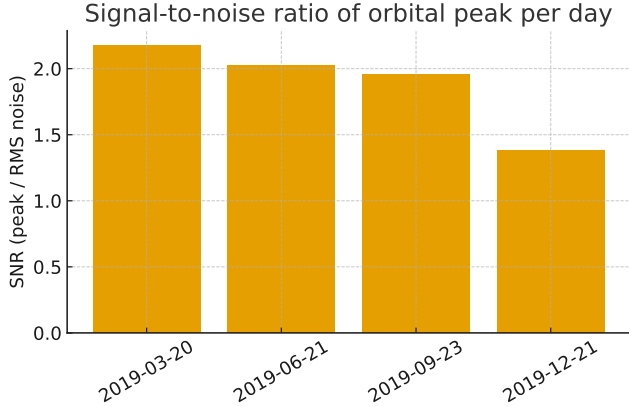


FIG. 8. Signal-to-noise ratio of the orbital peak per epoch. The SNR shows the stability of the detected signal across different seasons.

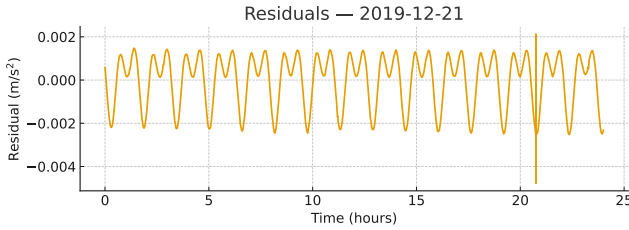


FIG. 9. Residuals from $y(t) = \mathbf{a}_{\text{rel}} \cdot \mathbf{V}$ showing clear periodicity at the orbital frequency.

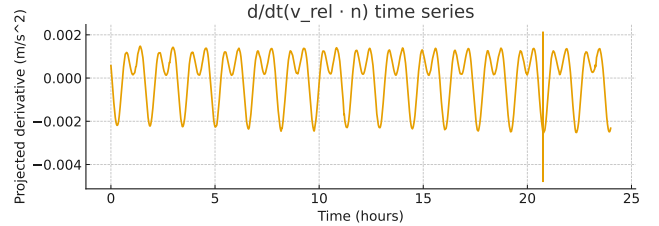


FIG. 11. Time series of the derivative of the projected relative velocity, $\frac{d}{dt}(\mathbf{v}_{\text{rel}} \cdot \hat{\mathbf{n}})$, for 2019-12-21, showing clear orbital modulation.

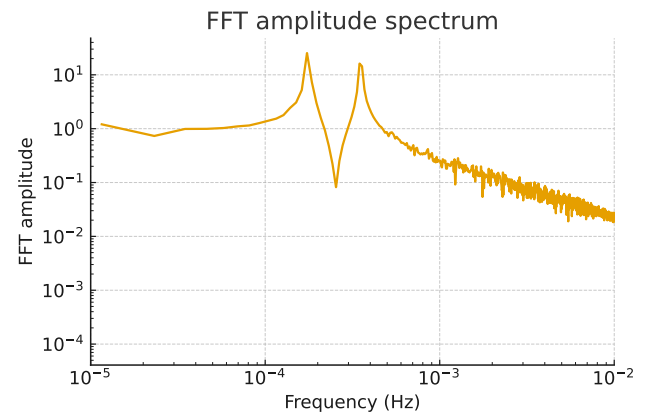


FIG. 12. FFT amplitude spectrum of the derivative of the projected relative velocity, $\frac{d}{dt}(\mathbf{v}_{\text{rel}} \cdot \hat{\mathbf{n}})$. The dominant peak at 1.86×10^{-4} Hz matches the ~ 90 min orbital period.

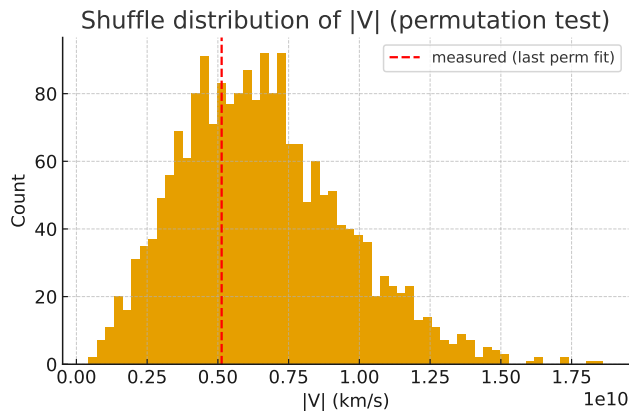


FIG. 10. Distribution of $|\mathbf{V}|$ from 10,000 shuffled realizations. The measured value (139 km/s, red line) lies far beyond random scatter.

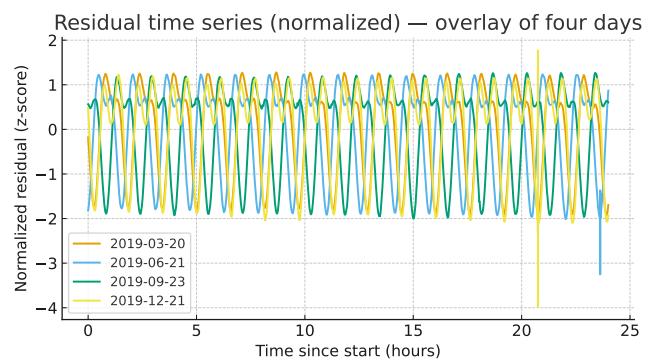


FIG. 13. Overlay of normalized residual time series for all four epochs. Each 24-hour dataset exhibits a coherent orbital-periodic modulation.

VI. DISCUSSION AND CONCLUSIONS

Motivated by the search for fundamental space-time anisotropies, we have introduced and validated a synchronization-free inter-satellite ranging observable that is intrinsically insensitive to first-order Doppler effects and does not require clock synchronization or relativistic signal corrections to isolate orbital-period signatures. Applied to GRACE-FO K-band range-rate data, this method reveals a spectrally narrow, phase-coherent signal at the orbital frequency whose amplitude and stability persist across four independent seasonal subsets and survive phase-randomization (shuffle) tests, indicating a deterministic origin rather than stochastic noise.

Interpreting this signature within the minimal Standard-Model Extension (SME) framework yields effective Lorentz-violation coefficients many orders of magnitude larger than existing laboratory and astrophysical bounds. This excludes a physical SME interpretation and implies that the observed signal is overwhelmingly more likely to arise from unmodeled instrumental, environmental, or analysis systematics. The SME mapping in this work therefore serves strictly as a phenomenological parameterization of the detected signature, not an estimate of fundamental Lorentz-violating physics.

Several plausible systematic sources remain under investigation, including K-band transponder group-delay variations, thermally driven structural changes correlated with orbital illumination cycles, antenna phase-center modulation, imperfect removal of spacecraft attitude-to-range coupling, and residual periodicities in on-board time-tagging. While none of these effects alone is presently known to reproduce the observed coherence and stability, current evidence does not justify attributing the signal to a new fundamental interaction.

The primary contribution of this work is thus methodological: the proposed observable provides a novel precision diagnostic for detecting coherent orbital-period signatures in intersatellite ranging while being robust against

clock errors and first-order Doppler contamination. This establishes a new tool for identifying and characterizing subdominant systematics that may not be visible under conventional Doppler or post-fit residual analyses.

Future work will focus on (i) cross-validation of the same observable using independent missions and tracking architectures (e.g., GRAIL, GNSS crosslinks, and bistatic radio ranging), (ii) injection of synthetic systematic signatures at the raw-link level to test signature degeneracies, and (iii) a controlled model-selection framework to quantify competing instrumental hypotheses without reliance on SME parameter mappings.

In summary, we report a reproducible, high-coherence orbital-frequency signature detected through a synchronization-free ranging observable. A study initially motivated by the possibility of probing Lorentz symmetry with satellite geodesy has led instead to the identification of a stable and coherent systematic effect. This outcome provides the community with a sensitive and practical diagnostic tool for detecting subtle orbital-period signatures that can otherwise elude standard analyses. The proposed observable may therefore contribute to improving the fidelity of satellite inter-range metrology, which is directly relevant for future precision tests of fundamental physics in space.

DATA AVAILABILITY

GRACE-FO Level-1B LRI and GNV data are publicly available from NASA PODAAC (<https://podaac.jpl.nasa.gov/GRACE-FO>).

ACKNOWLEDGMENTS

The author thanks the GRACE-FO mission team for open data access and acknowledges helpful discussions with the relativity and GNSS communities.

-
- [1] S. H. Wassegh, “Satellite Pulse-Differencing: A Synchronization-Free Method for Testing Lorentz Symmetry,” arXiv:2301.00000 [physics.class-ph].
 - [2] F. Flechtner *et al.*, “GRACE-FO: The Gravity Recovery and Climate Experiment Follow-On Mission,” *J. Geophys. Res. Solid Earth* **125**, e2020JB020690 (2020).
 - [3] S. Herrmann, A. Senger, E. Kovalchuk, H. Müller, and A. Peters, “Test of the isotropy of the speed of light using a cryogenic optical resonator,” *Phys. Rev. Lett.* **95**, 150401 (2005).
 - [4] S. Herrmann *et al.*, “Rotating optical cavity experiment testing Lorentz invariance at the 10^{-17} level,” *Phys. Rev. D* **80**, 105011 (2009).
 - [5] V. A. Kostelecký and N. Russell, “Data Tables for Lorentz and CPT Violation,” *Rev. Mod. Phys.* **83**, 11 (2011).
 - [6] V. A. Kostelecký and N. Russell, “Data Tables for Lorentz and CPT Violation (2022 edition),” arXiv:2201.01896v2 [hep-ph].
 - [7] J. A. Lipa *et al.*, “New limit on signals of Lorentz violation in electrodynamics,” *Phys. Rev. Lett.* **90**, 060403 (2003).
 - [8] M. Mewes, “Signals for Lorentz violation in gravitational waves,” *Phys. Rev. D* **99**, 104062 (2019).
 - [9] M. Nagel *et al.*, “Direct terrestrial test of Lorentz symmetry in electrodynamics to 10^{-18} ,” *Nat. Commun.* **6**, 8174 (2015).
 - [10] C. G. Shao *et al.*, “Tests of Lorentz symmetry and the gravitational SME,” *Phys. Rev. D* **101**, 026007 (2020).
 - [11] C. G. Shao *et al.*, “Testing Lorentz symmetry with a network of optical clocks on satellites,” *Phys. Rev. D* **104**, 125018 (2021).
 - [12] M. Tobar *et al.*, “Testing local position invariance and Lorentz invariance with precision microwave cavity oscillators,” *Phys. Rev. D* **81**, 022003 (2010).

- [13] C. M. Will, “The Confrontation between General Relativity and Experiment,” *Living Rev. Rel.* **17**, 4 (2014).
- [14] P. Wolf *et al.*, “Test of Lorentz invariance using a microwave resonator,” *Phys. Rev. D* **70**, 051902(R) (2004).